SCIENCE CHINA
Technological Sciences

•Article•

https://doi.org/10.1007/s11431-023-2432-1

Memristive effects on an improved discrete Rulkov neuron model

BAO Han[1], LI KeXin[1], MA Jun[2], HUA ZhongYun[3], XU Quan[1] & BAO BoCheng[1*]

[1] *School of Microelectronics and Control Engineering, Changzhou University, Changzhou 213159, China;*
[2] *Department of Physics, Lanzhou University of Technology, Lanzhou 730050, China;*
[3] *School of Computer Science and Technology, Harbin Institute of Technology, Shenzhen, Shenzhen 518055, China*

Received March 31, 2023; Accepted May 16, 2023; published online September 26, 2023

A change in neuronal-action potential can generate a magnetically induced current during the release and propagation of intracellular ions. To better characterize the electromagnetic-induction effect, this paper presents an improved discrete Rulkov (ID-Rulkov) neuron model by coupling a discrete model of a memristor with sine memductance into a discrete Rulkov neuron model. The ID-Rulkov neuron model possesses infinite invariant points, and its memristor-induced stability effect is evaluated by detecting the routes of period-doubling and Neimark-Sacker bifurcations. We investigated the memristor-induced dynamic effects on the neuron model using bifurcation plots and firing patterns. Meanwhile, we theoretically expounded the memristor initial-boosting mechanism of infinite coexisting patterns. The results show that the ID-Rulkov neuron model can realize diverse neuron firing patterns and produce hyperchaotic attractors that are nondestructively boosted by the initial value of the memristor, indicating that the introduced memristor greatly benefits the original neuron model. The hyperchaotic attractors initially boosted by the memristor were verified by hardware experiments based on a hardware platform. In addition, pseudorandom number generators are designed using the ID-Rulkov neuron model, and their high randomness is demonstrated based onstrict test results.

neuron model, invariant point, memristive effect, complex dynamics, pseudorandom number generators

Citation: Bao H, Li K X, Ma J, et al. Memristive effects on an improved discrete Rulkov neuron model. Sci China Tech Sci, 2023, 66, https://doi.org/10.1007/s11431-023-2432-1

1 Introduction

Generally, neuronal electrical activity arises from high-dimensional dynamics of nonlinear processes [1]. These nonlinear processes cause generations and interactions of ionic currents to move in membrane channels [2]. To mathematically characterize these electrical activities, a number of theoretical neuron models that involve various nonlinearities were successively proposed in the past few decades. The Hodgkin-Huxley [2] and Morris-Lecar [3] models are two well-known neuron models that are based on the ion channels of biological neurons. These ion channels have been verified to be well simulated using memristors [3,4]. Owing to their nonlinearity and nonvolatility [5], memristors can be used to mimic neural synapses [6] or exhibit electromagnetic induction [7] during the interactions of extracellular and intracellular ions. In other words, when neuronal electrical activities are triggered, biophysical effects can be reliably demonstrated by introducing memristors into the neuron models.

Biological neurons can be stimulated to demonstrate a variety of firing patterns, and further cooperation among neurons is critical to induce mode transition and regulation of body gaits [2]. Most nonlinear circuits can be specially designed to reproduce similar dynamical properties in the membrane potential of biological neurons, and further involvement of specific electric components such as memristors, Josephson junctions, thermistors, and piezoelectric ceramics in the branch circuit can enhance the possible biophysical function of a neural circuit [5], which is devel-

*Corresponding author (email: mervinbao@126.com)

oped from known nonlinear circuits. As a result, each functional neural circuit can be considered a biological neuron, and these memristive, piezoelectric, and thermosensitive neural circuits can be designated as neuron-based neuromorphic circuits, which can encode and process physical signals as artificial and biological neurons [8].

The physical attributes (charge and flux) of a memristor enable it to become a special nonlinear component with an inherent state in the voltage-current domain [4]. A flux-controlled memristor introduces the effect of resistance and magnetic field, an inherent state that predicates its memory ability associated with the intrinsic memory characteristic of a magnetic field. Thus, memristive nonlinearity involves an inherent state that introduces a physical effect, which is different from conventional nonlinearity [9]. Owing to their unique nonlinearity, memristors have been broadly used in neuron-based neuromorphic circuits, and their dynamic dependence on the initial value of a memristive variable, known as the memristive effect, has attracted great attention [10,11]. By applying a controllable mask process, a parallel dynamic memristor-based reservoir computing system was reported in [12], which achieved highly efficient computing to process temporal signals. Finite-time stabilization of memristor-based inertial neural networks with time-varying delays was investigated in [13] using a novel reliable control strategy. A memristor-based neural circuit was designed by simulating the short-term facilitation and long-term potentiation to demonstrate the neurochemical learning and memory foundations in [14]. Furthermore, Kumar et al. [15] showed that the Hopfield computing network could more efficiently and accurately converge to a solution when incorporated with memristors. Lin et al. [16] programmed parallel operation kernels into a three-dimensional (3D) array by constructing a 3D memristor circuit and implemented a complex neural network with software-comparable accuracy in recognizing handwritten digits. Bilotta et al. [17] confirmed that when memristors were embodied, a cellular neural network could achieve better performance in pattern recognition and image processing. Consequently, memristors have become an important component of neuron-based neuromorphic circuits and have received great attention.

Neuronal action potentials can trigger electromagnetic induction [18]. When neuronal electrical activities are associated with electromagnetic induction, a memristor-based neuron model has been presented to describe the electromagnetic-induction effect [19]. Recently, several novel memristive neuron models have been developed by coupling memristors with existing neuron models, and memristor effects with complex firing patterns have been revealed [20,21]. However, most previous studies mainly focused on continuous models of memristive neurons. Establishing a memristor-based discrete neuron model and studying its memristive effect on complex firing patterns are challenging. More lately, a discrete model of memristor has been presented by discretizing a continuous model of memristor [22]; several simple memristive maps have been constructed, and their complex dynamical behaviors were disclosed in terms of hyperchaotic oscillation, coexisting attractors, and period-doubling or quasiperiodic bifurcation [23,24]. Encouraged by this strategy, we propose a discrete memristive Rulkov neuron model [11] using a discrete memristor and a two-dimensional (2D) neuron map [25] for the first time. Thus, the memristor-induced electromagnetic-induction effects have been simulated in the proposed neuron model, and the actual electrical activities of biological neurons have been represented when involved with the biophysical memory effect.

Some of the previous work preferred to mimic neural activities using continuous dynamic equations, and a continuous memristor was involved in estimating the effect of electromagnetic induction and radiation [18–21]. In fact, spiking and bursting neurons trigger firing patterns at certain intervals, and multiple firing modes in electrical activities are developed rather than kept in continuous firing patterns. In the presence of external electric stimuli and electromagnetic fields, continuous firing activities can be suppressed at certain intervals, and the inner electromagnetic field may remain invariant within these intervals. Therefore, a discrete neuron model coupled with a discrete memristor term can be more suitably employed to approach the physical process of electrical activities [11].

The Rulkov neuron model in [26,27] is a simple 2D map that generates chaotic bursting similar to biological neurons. Here, the nonlinearity used is smooth and continuous, whereas that used in [25] was nonsmooth and discontinuous. To achieve the memristor initial-boosting behavior in [23], an improved discrete Rulkov (ID-Rulkov) neuron model is developed by coupling a memristor with a sine memductance used in [23] into a simple 2D map model presented in [26,27]. Because of the introduction of the memristor with periodic memductance, the constructed ID-Rulkov neuron model can generate diverse firing patterns of neurons and produce hyperchaotic attractors that are nondestructively boosted by the memristor initial value [28]. Notably, such memristor initial-boosting behavior has not been reported in existing discrete neuron models. In particular, because the ID-Rulkov neuron model exhibits better performance than many existing chaotic maps, its generated hyperchaotic sequences are more suitable for various chaos-based industrial applications [23].

The main contributions and novelty of the present study are outlined as follows. (1) To better describe the electromagnetic-induction effect, we propose an ID-Rulkov neuron model with infinite invariant points and evaluate the memristor-induced stability effects by detecting the period-doubling and Neimark-Sacker bifurcations. (2) We theoretically

expound the memristor initial-boosting mechanism of infinite coexisting patterns and numerically investigate the memristor-induced dynamical effects on the ID-Rulkov neuron model. (3) We design pseudorandom number generators (PRNGs) using the ID-Rulkov neuron model. The pseudo-random numbers (PRNs) feature high randomness and are suitable for many chaos-based applications.

2 Discrete modeling for neurons considering electromagnetic induction

As demonstrated by neurobiological experiments and numerical simulations, an individual neuron can show irregular bursts. This study provides an example to show the electromagnetic-induction effects of hyperchaotic dynamics of bursts on a chaotically bursting cell when the electromagnetic induction triggered by action potential is considered.

2.1 Proposed ID-Rulkov neuron model

A memristor is a nonlinear circuit element with an inherent state. It is different from conventional nonlinear circuit elements [9]. By referring to the memristor discrete modeling strategy in [22,23], a discrete memristor with sine memductance can be developed and expressed as

$$\begin{cases} i_n = v_n \sin(\varphi_n), \\ \varphi_{n+1} = \varphi_n + \varepsilon v_n, \end{cases} \tag{1}$$

where n represents the iteration associated with time, variables v_n, i_n, and φ_n stand for the sampling values of $v(t)$, $i(t)$, and $\varphi(t)$ at the nth iteration, respectively, and ε is a positive constant representing the scale factor of time. When a discrete sinusoidal voltage is applied to the memristor, the fingerprints of the pinched hysteresis loops, the memory effect related to the initial value, and local activity can be demonstrated by numerical simulations [23]. We note that the memductance in eq. (1) is periodically multivalued, whereas that in [11] is single-valued with a threshold. In addition, the discrete memristor model given in eq. (1) is an ideal memristor model [4], which is intrinsically distinct from physical memristive devices [29,30].

The Rulkov model presented in [26] is a simple 2-D map and is established under a dynamical assumption. It is different from the Hodgkin-Huxley [2], Morris-Lecar [3], and Chay [31] models derived from biophysical mechanisms. The Rulkov model can generate chaotic bursting behavior that is similar to that of biological neurons. It can be expressed as

$$\begin{cases} x_{n+1} = \alpha / \left(1 + x_n^2\right) + y_n, \\ y_{n+1} = y_n - \sigma x_n - \beta, \end{cases} \tag{2}$$

where x_n is the fast dynamical variable that denotes the neuronal-action potential, y_n is the slow variable representing the recovery variable, α and σ are positive control parameters, and β is the external influence. We need to note that the nonlinearity $F(x_n, \alpha) = 1/(1 + x_n^2)$ used in eq. (2) is smooth and continuous, whereas that used in [25] is non-smooth and discontinuous. The smooth and continuous nonlinearity makes feasible stability analysis of the invariant point of the discrete map.

Changes in the neuronal-action potential during the release and propagation of intracellular ions can generate a magnetically induced current. To better characterize the electromagnetic-induction effect, an ID-Rulkov neuron model can be built by coupling the memristor presented in eq. (1) to the original discrete Rulkov neuron model given in eq. (2). The structure of the proposed ID-Rulkov neuron model is shown in Figure 1 in which $F(x_n, \alpha)$ and σ are the nonlinear term and control parameter used in eq. (2), respectively, and k is the memristor gain. The ID-Rulkov neuron model can be easily derived using such a structure, and its mathematical representation is expressed as

$$\begin{cases} x_{n+1} = \alpha / (1 + x_n^2) + y_n + k x_n \sin(\varphi_n), \\ y_{n+1} = y_n - \sigma x_n, \\ \varphi_{n+1} = \varphi_n + \varepsilon x_n. \end{cases} \tag{3}$$

We note that the external influence should be set to $\beta = 0$; otherwise, the aforementioned discrete model tends to have unbounded behavior. In particular, $k x_n \sin(\varphi_n)$ estimates the equivalent induction current from the memristive channel. The biophysical mechanism is considered an electromagnetic-induction effect in which intracellular and extracellular ions are pumped and propagated to generate time-varying channel current and magnetic field. As a result, this induction current can alter the excitability of the neuron as external stimuli. The typical values and variable ranges of each parameter in the ID-Rulkov neuron model given in eq. (3) are listed in Table 1 for easy reference.

From a biological standpoint, the media and cell can be successively magnetized and polarized in the presence of an external electromagnetic field, and continuous fluctuations

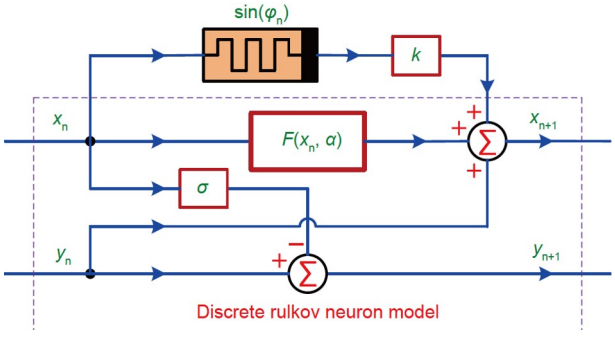

Figure 1 (Color online) Structure of the ID-Rulkov neuron model.

Table 1 Typical values and variable ranges of each parameter in eq. (3)

Parameters	Physical meanings	Values
α	Parameter in the original model	5
σ	Parameter in the original model	0.2
ε	Scale factor in the memristor	0.3
k	Memristor gain (variable)	[−1.6, 1.6]
$\mu(\varphi_0)$	Memristor initial value (variable)	[−π, π] or [−4π, 3π]

of the electromagnetic field may induce a periodic induced current in the flexible media [8,32]. In particular, periodic firing can modulate the propagation, pumping, and distribution of intracellular ions in the cell. Thus, a memristor with periodic memductance can be applied to simulate the polarization characteristics.

2.2 Proposed ID-Rulkov neuron model

The stability of a discrete dynamical system can be characterized by its invariant point. An invariant point of a discrete map is defined as the point that maps to itself in its domain [23]. Thus, the invariant point of the ID-Rulkov neuron model given in eq. (3) represents the solutions of the following equations:

$$\begin{cases} X = \alpha/(1+X^2) + Y + kX\sin(\psi), \\ Y = Y - \sigma X, \\ \psi = \psi + \varepsilon X. \end{cases} \tag{4}$$

According to the second or third equation in eq. (4), $X = 0$. Substituting $X = 0$ into the first equation in eq. (4) yields $Y = -\alpha$. Because $X = 0$, the first equation in eq. (4) is true for any real constant of ψ. Hence, the invariant point of the ID-Rulkov neuron model can be obtained from eq. (4) as

$$P = (X, Y, \psi) = (0, -\alpha, \mu), \tag{5}$$

where μ is a constant that depends on the initial position on the φ axis. In other words, any point on the φ axis is an invariant point, which indicates that the ID-Rulkov neuron model in eq. (3) has infinite invariant points in the φ axis.

An invariant point has a stable or unstable state, and its stability is reflected by its Jacobian eigenvalues. The Jacobian of the ID-Rulkov neuron model at $P = (0, -\alpha, \mu)$ is calculated as

$$\mathbf{J}_S = \begin{bmatrix} k\sin\mu & 1 & 0 \\ -\sigma & 1 & 0 \\ \varepsilon & 0 & 1 \end{bmatrix}. \tag{6}$$

The eigenvalues of the Jacobian in eq. (6) are solved as

$$\begin{aligned} &\lambda_1 = 1, \\ &\lambda_{2,3} = 0.5 + 0.5M \pm \sqrt{0.25(1+M)^2 - \sigma - M}, \end{aligned} \tag{7}$$

where $M = k\sin\mu$. Here, the newly introduced parameter M is determined by gain k and initial value μ, which are both associated with the memristor. For convenience, we define parameter M as a memristor parameter. Thus, the Jacobian eigenvalues are closely dependent on memristor parameter M and positive parameter σ but completely independent of positive scale factor ε.

Obviously, if $|\lambda_2| < 1$ and $|\lambda_3| < 1$, invariant point P is critically stable because $|\lambda_1| = 1$; otherwise, it is unstable. We denote memristor parameter M as a variable parameter and specify the representative parameter setting as $\sigma = 0.2$. From eq. (7), we obtain the critical stable interval of M as

$$-1.1 < M < 0.8. \tag{8}$$

When M increases within [−1.2, −1] and [0.7, 0.9], the loci of the three Jacobian eigenvalues in eq. (7) are shown in Figure 2(a) and (b), respectively. Therefore, λ_1 is a critical root and is always on the unit circle. However, λ_2 and λ_3 can be either inside or outside the unit circle depending on M. When M increases from −1.2 to −1, λ_2 is located inside the unit circle, but λ_3 crosses the unit circle from −1, leading to the occurrence of period-doubling bifurcation at $M = -1.1$. When M increases from 0.7 to 0.9, complex conjugate roots λ_2 and λ_3 simultaneously go through the unit circle from the first and fourth quadrants, respectively, resulting in the appearance of Neimark-Sacker bifurcation at $M = 0.8$.

In summary, if memristor parameter M is located in the region given by eq. (8), the ID-Rulkov neuron model is critically stable. When M changes, the ID-Rulkov neuron model follows the routes of period-doubling and Neimark-Sacker bifurcations. Because $|\lambda_1| = 1$, the memristor-induced stability effect on the ID-Rulkov neuron model cannot be determined from eq. (8). However, it can be effectively detected using numerical simulations.

3 Memristor-induced dynamic effects

This section presents our investigation of the memristor-induced dynamical effects on the ID-Rulkov model with variable memristor parameters k and φ_0. The other parameters are fixed at $\alpha = 5$, $\sigma = 0.2$, $\varepsilon = 0.3$, and initial values $(x_0, y_0) = (0, 0)$. The mixed 2D bifurcation diagram is illu-

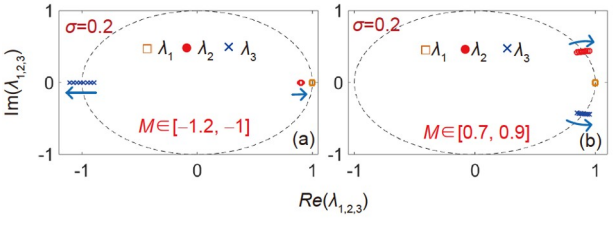

Figure 2 (Color online) Loci of three Jacobian eigenvalues with the increase in M at fixed $\sigma = 0.2$. (a) $M \in [-1.2, -1]$; (b) $M \in [0.7, 0.9]$.

strated by calculating the spike periodicities of action potential x per cycle, and the maximal Lyapunov exponent (MLE) plot is measured using Wolf's Jacobian-based method [23].

3.1 Memristor parameter-related dynamics

The mixed 2D bifurcation diagram can be used to describe the memristor parameter-related dynamical distributions in the parameter plane. When the memristor parameters are varied within $\varphi_0 \in [-\pi, \pi]$ and $k \in [-1.6, 1.6]$, the mixed 2D bifurcation diagram in the φ_0-k plane can be generated, as shown in Figure 3(a). The parameter planes that emerge from the orbits are drawn by different colors according to different spike periodicities. Yellow represents hyperchaos (denoted as HC), brown represents chaos (denoted as CH), pink represents multiple periods with cycle numbers greater than eight (denoted as MP), and the other colors represent Period-1 to Period-8, which are denoted as P1 to P8, respectively. We can observe that the color-painted regions in Figure 3(a) mainly consist of brown (Chaos), black (Period-2), yellow (Hyperchaos), and blue (Period-3). In addition, we can observe numerous periodic windows with tangent bifurcations and routes to chaos with period-doubling bifurcations in the parameter plane.

The mixed 2-D MLE plot can also be used to illustrate the memristor parameter-related dynamical distributions in the parameter plane. The mixed 2D MLE plot in the φ_0-k plane is shown in Figure 3(b) using the same memristor parameter regions shown in Figure 3(a). In the same manner, the parameter planes that emerge from the orbits are drawn by different colors according to the different MLE values. The red-yellow color denotes chaos due to positive MLE, and the black color denotes the period labeled due to zero MLE. Comparison of Figure 3(a) and (b) reveals that the dynamic distributions described by different measures are completely consistent. Therefore, the numerical results in Figure 3 show that the coupled memristor can induce complex dynamical effects on the ID-Rulkov neuron model.

Subsequently, we take six sets of memristor parameters from the different colorful regions in Figure 3 to demonstrate the firing patterns generated from the ID-Rulkov neuron model. Figure 4 shows the iterative sequences of variables x, y, and φ for different sets of memristor parameters. From the photographs shown in Figure 4, various periodic, chaotic, and hyperchaotic spiking/bursting firing patterns are revealed in the ID-Rulkov neuron model. Three Lyapunov exponents (LEs) of these firing patterns can be calculated, and the results are listed in Table 2. We note that no positive LEs exist for the periodic firing pattern, one positive LE for the chaotic firing pattern, and two positive LEs for the hyperchaotic firing pattern. Consequently, the ID-Rulkov neuron model exhibits complex dynamics, and its firing patterns closely rely on its memristor parameters.

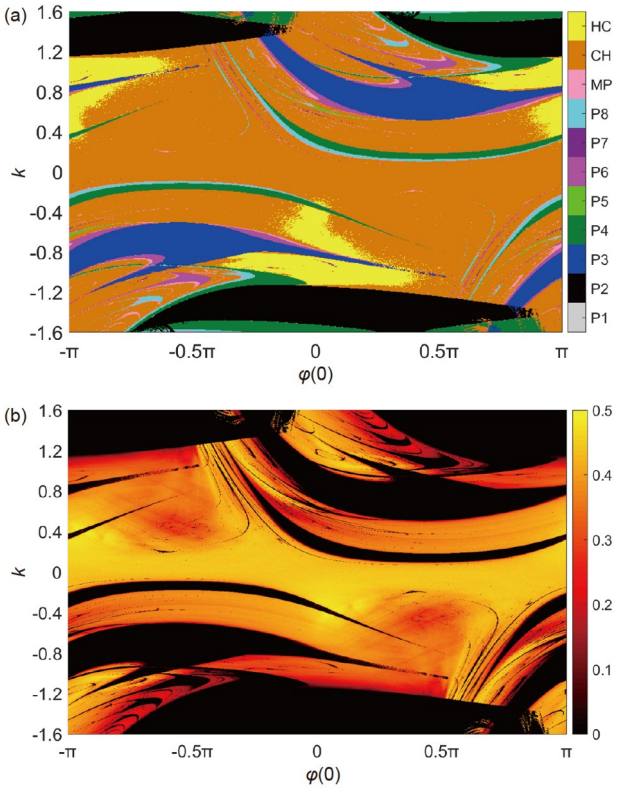

Figure 3 Memristor parameter-related dynamical distributions in the φ_0-k plane at fixed $\alpha = 5$, $\sigma = 0.2$, $\varepsilon = 0.3$, and $(x_0, y_0) = (0, 0)$. (a) 2D bifurcation diagram obtained by calculating the spike periodicities per cycle; (b) 2D MLE plot measured using Wolf's Jacobian-based method.

According to the memristor parameter-related dynamical distributions shown in Figure 3, we can obtain the memristor parameter-related LE spectra and bifurcation diagrams, which are shown in Figure 5. We only partially display the third LE spectra for better visual effects.

First, the memristor initial value is fixed at $\varphi_0 = 0$, and the memristor gain is adjusted within $k \in [-1.6, 1.6]$. The top of Figure 5(a) shows the LE spectra, whereas the bottom of Figure 5(a) shows the bifurcation diagram of action potential x. We can observe that with the evolution of k, the ID-Rulkov model undergoes periodic spiking with zero MLE, hyperchaotic spiking with the first two positive LEs, and chaotic spiking with one positive LE. The hyperchaotic behavior is located within $k \in [-1.135, -0.858]$ and $k \in [-0.761, -0.371]$. In addition, the reverse and forward period-doubling bifurcations, tangent bifurcations, and periodic windows can be found within the evolution range of k, which leads to the appearance of complex dynamics.

Second, the memristor gain is fixed at $k = -1$, and the memristor initial value is varied within $\varphi_0 \in [-\pi, \pi]$. The memristor initial-value-related LE spectra (top) and bifurcation diagram of action potential x (bottom) are shown in Figure 5(b), which shows that following the increase in φ_0,

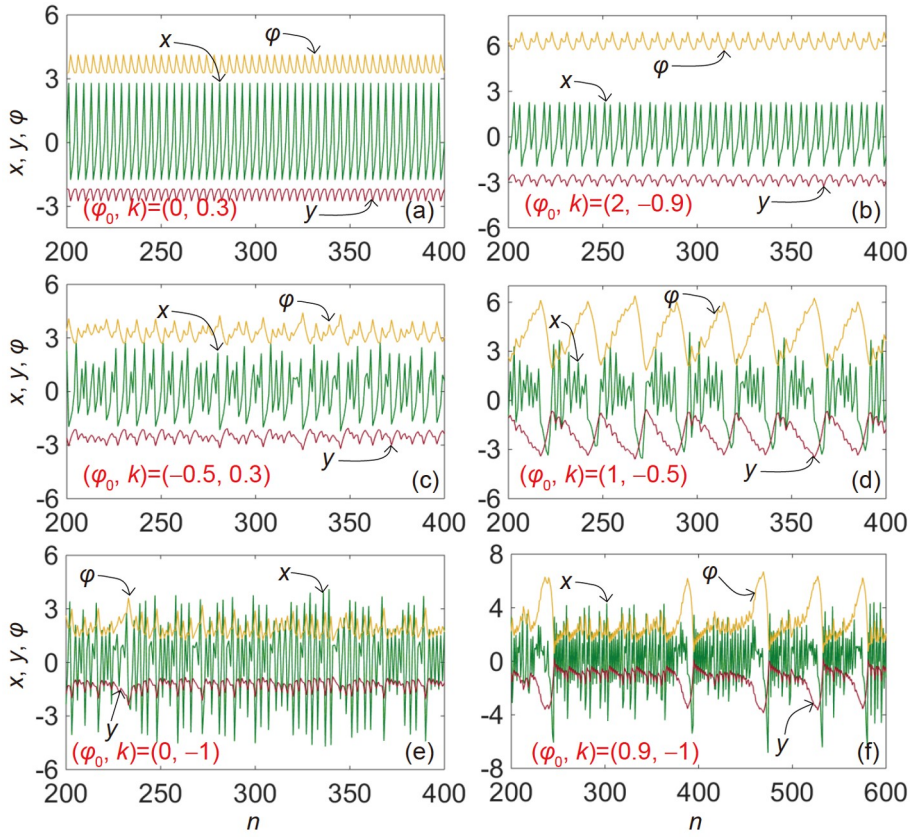

Figure 4 Memristor parameter-related firing patterns of variables x, y, and φ in the ID-Rulkov neuron model. (a) Periodic spiking at $(\varphi_0, k) = (0, 0.3)$; (b) periodic bursting at $(\varphi_0, k) = (2, -0.9)$; (c) chaotic spiking at $(\varphi_0, k) = (-0.5, 0.3)$; (d) chaotic bursting at $(\varphi_0, k) = (1, -0.5)$; (e) hyperchaotic spiking at $(\varphi_0, k) = (0, -1)$; (f) hyperchaotic bursting at $(\varphi_0, k) = (0.9, -1)$.

Table 2 Firing patterns and LEs of the six sets of memristor parameters

(ϕ_0, k)	Firing patterns	(LE_1, LE_2, LE_3)
(0, 0.3)	Periodic spiking	(−0.0004, −0.0921, −0.9115)
(2, −0.9)	Periodic bursting	(−0.0001, −0.1935, −0.1940)
(−0.5, 0.3)	Chaotic spiking	(0.4217, 0.0000, −0.2703)
(1, −0.5)	Chaotic bursting	(0.3353, 0.0000, −0.0974)
(0, −1)	Hyperchaotic spiking	(0.3117, 0.0398, −0.0000)
(0.9, −1)	Hyperchaotic bursting	(0.3313, 0.0181, −0.0010)

the ID-Rulkov neuron model exhibits periodic spiking with zero MLE, hyperchaotic spiking with the first two positive LEs, and chaotic spiking with one positive LE. The hyperchaotic behavior appears within $k \in [-0.697, 1.148]$. Further, the reverse and forward period-doubling bifurcations, tangent bifurcations, and periodic windows can be observed as φ_0 increases from $-\pi$ to π. The memristor initial-value-related dynamical behavior indicates the coexistence of infinite firing patterns, i.e., the emergence of extreme multistability.

3.2 Dynamics boosted by memristor initial value

The proposed ID-Rulkov neuron model contains infinite invariant points that are closely associated with the memristor initial value. The infinite invariant points can cause the emergence of infinite coexisting attractors due to the memristor initial boosting.

To expound the boosting mechanism due to the memristor initial value, the ID-Rulkov neuron model in eq. (3) can be rewritten as

$$\begin{cases} x_{n+1} = \alpha / \left(1 + x_n^2\right) + y_n + k x_n \sin\left(\varphi_0 + \sum_{m=0}^{n-1} x_m\right), \\ y_{n+1} = y_n - \sigma x_n. \end{cases} \tag{9}$$

We denote a linear conversion as

$$\varphi_0 = \varphi_{00} + 2m\pi, \tag{10}$$

where m is an integer and φ_{00} is the initial value within $[-\pi, \pi]$ and satisfies the following condition:

$$-\pi < \varphi_{00} + \sum_{m=0}^{n-1} x_m < \pi. \tag{11}$$

Hence, we obtain

$$\sin\left(\varphi_0 + \sum_{m=0}^{n-1} x_m\right) = \sin\left(\varphi_{00} + \sum_{m=0}^{n-1} x_m\right). \tag{12}$$

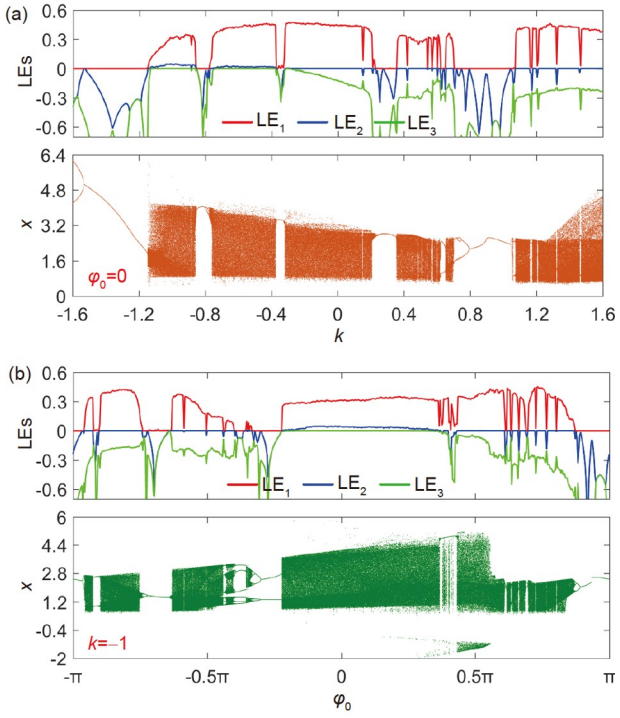

Figure 5 Memristor parameter-related bifurcation behavior when the memristor gain and memristor initial value vary in their determined regions. (a) Memristor gain-related (bottom) bifurcation diagram and LE (top) spectra at fixed $\varphi_0 = 0$; (b) memristor initial-value-related (top) LE spectra and (bottom) bifurcation diagram at fixed $k = -1$.

The result shown in eq. (12) indicates that the sine memductance in eq. (1) has a cyclic property.

Therefore, the discrete map-based ID-Rulkov neuron model in eq. (9) is cyclic at the memristor initial value φ_0. The cyclic property is confirmed by the invariance of eq. (9) using the linear conversion in eq. (10). This result demonstrates that the dynamics of the ID-Rulkov neuron model can be reproduced as memristor initial value φ_0 periodically evolves with fixed 2π offset. As a result, the ID-Rulkov neuron model can be boosted, and its firing patterns can be boosted by the memristor initial value along the φ axis.

To demonstrate the cyclic property of the ID-Rulkov neuron model, we use the mixed 2D bifurcation diagram to illustrate the dynamical distributions in the parameter plane. Memristor initial value φ_0 is varied in $[-4\pi, 3\pi]$, which covers three full 2π cycles, and memristor gain k is varied within $[-1.6, 1.6]$, which is the same as that shown in Figure 3(a). The mixed 2D bifurcation diagram in the φ_0-k plane is shown in Figure 6 using the same method shown in Figure 3(a). We note that the painted colors and their marks are the same as those shown in Figure 3(a). We can observe that when the memristor initial value φ_0 periodically evolves with fixed offset 2π, the ID-Rulkov neuron model can reproduce the complex dynamics within the main value interval $[-\pi, \pi]$ of the memristor initial value, leading to the occurrence of memristor initial-boosting behavior.

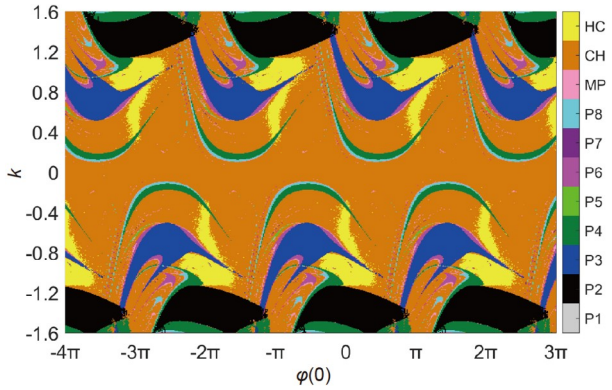

Figure 6 Memristor parameter-related dynamical distributions indicated by 2D bifurcation diagram in the φ_0-k plane when φ_0 is varied in $[-3\pi, 4\pi]$ and k is varied in $[-1.6, 1.6]$ for fixed $\alpha = 5$, $\sigma = 0.2$, $\varepsilon = 0.3$, and $(x_0, y_0) = (0, 0)$.

We consider $k = -0.5$ and $\varphi_0 \in [-4\pi, 3\pi]$ as examples. The memristor initial-value-related LE spectra (top) and bifurcation diagram of action potential x (bottom) are shown in Figure 7. We can obviously see that the dynamical behavior within $\varphi_0 \in [-3\pi, -\pi]$ and $\varphi_0 \in [\pi, 3\pi]$ is the same as that within $\varphi_0 \in [-\pi, \pi]$. The results demonstrate that the infinite coexisting patterns can be boosted by the memristor initial value with fixed offset 2π.

According to the results shown in Figure 7, the iteration sequences provided by the ID-Rulkov neuron model are boosted in their dynamic amplitudes by the memristor initial values with period 2π. We denote the representative parameter and initial settings as $\alpha = 5$, $\sigma = 0.2$, $\varepsilon = 0.3$, $k = -0.5$, and $(x_0, y_0) = (0, 0)$. When four sets of memristor initial values are set to $\varphi_0 = 2l\pi$ ($l = -2, -1, 0, 1$), the generated hyperchaotic attractors are shown in Figure 8, which shows that all hyperchaotic attractors have similar fractal structures, and they can be controlled in the dynamic amplitudes by boosting the memristor initial values.

The performance metrics of the memristor initial-value-boosting hyperchaotic attractors shown in Figure 8 are evaluated using three LEs (LE_1, LE_2, and LE_3), spectral

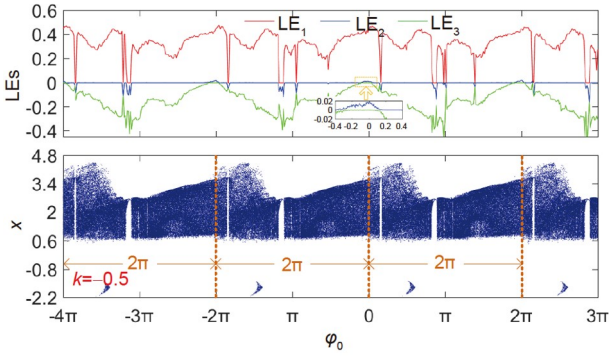

Figure 7 Memristor initial-value-related (top) LE spectra and (bottom) bifurcation diagram at fixed $k = -0.5$, which demonstrate the infinite coexisting patterns boosted by the memristor initial value with fixed 2π offset.

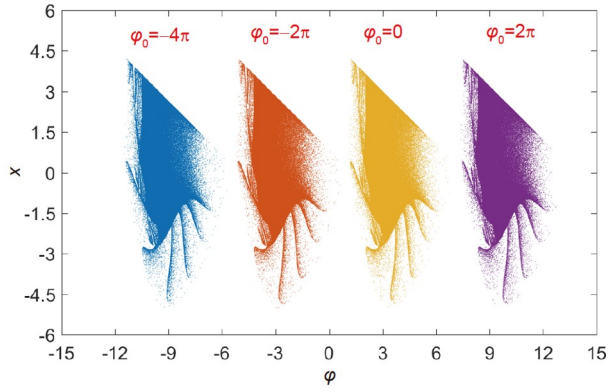

Figure 8 Memristor initial-boosted hyperchaotic attractors of the ID-Rulkov neuron model for $\alpha = 5$, $\sigma = 0.2$, $\varepsilon = 0.3$, $k = -0.5$, and $(x_0, y_0) = (0, 0)$, which demonstrate the amplitude-controllable hyperchaos boosted by the memristor initial value.

entropy (SpecEn) [33], permutation entropy (PermEn) [34], and correlation dimension (CorDim) [35]. The calculation results are listed in Table 3. We can observe that the hyperchaotic attractors contain two large positive LEs, which indicate hyperchaos with outstanding performance metrics. Most importantly, these hyperchaotic attractors exhibited nearly identical performance metrics, and the slight difference is caused by numerical-simulation errors. Therefore, the hyperchaotic attractors generated by the ID-Rulkov neuron model can be nondestructively boosted by the initial value of the memristor, which is applicable to various chaos-based information-engineering applications.

3.3 Experimental verification using hardware platform

The hyperchaotic attractors shown in Figure 8 contain iterative sequences in two dimensions. When the hyperchaotic sequences are used in industrial applications, we need to acquire them from a hardware platform. Owing to sinusoidal and reciprocal quadratic nonlinearities, the microcontroller-based digital circuit can more easily implement the ID-Rulkov neuron model than the discrete component-based analog circuit.

The hardware platform developed in [24] is directly adopted, and it is designed based on a 32-bit microcontroller with two digital-to-analog converters and some peripheral circuits. According to the ID-Rulkov neuron model in eq. (3), we program the model using the C language and download the code to the microcontroller. The parameters and initial values shown in Figure 8 are preloaded into the hardware platform, and the experimental results are physically captured by an oscilloscope.

When the power supply is turned on, the developed hyperchaotic attractors in the two-channel mode can be synchronously displayed by the oscilloscope, as shown in Figure 9. Four hyperchaotic attractors are shown to experimentally emerge within different amplitude ranges, and they can be nondestructively controlled by the memristor initial value with fixed offset 2π, indicating the feasibility of the digitally circuit-implemented platform for the ID-Rulkov neuron model.

Table 3 Performance metrics for the memristor initial-value-boosting hyperchaotic attractors

ϕ_0	(LE_1, LE_2, LE_3)	SpecEn	PermEn	CorDim
−4π	(0.4476, 0.0165, 0.0000)	0.9360	4.4386	1.7582
−2π	(0.4438, 0.0162, 0.0000)	0.9350	4.4241	1.7450
0	(0.4455, 0.0163, 0.0000)	0.9347	4.4334	1.7381
2π	(0.4448, 0.0171, 0.0000)	0.9340	4.3915	1.7266

4 Applications in PRNG

Chaotic systems have various applications, such as in PRNG [36]. To demonstrate the application of the ID-Rulkov neuron model in PRNG, we design four PRNGs using the generated hyperchaotic sequences and measure the randomness of the generated PRNs. We note that the hyperchaotic sequences are numerically generated by the ID-Rulkov neuron model using MATLAB software.

4.1 PRNG design

PRNG can be designed to illustrate the application of the ID-Rulkov neuron model. Let us denote hyperchaotic sequence $X = \{X(1), X(2), \ldots, X(n), \ldots\}$ as the hyperchaotic sequence of the neuronal-action potential under the same parameter and initial-value settings shown in Figure 8. New hyperchaotic sequence $Y = \{Y(1), Y(2), \ldots, Y(n), \ldots\}$ within the range

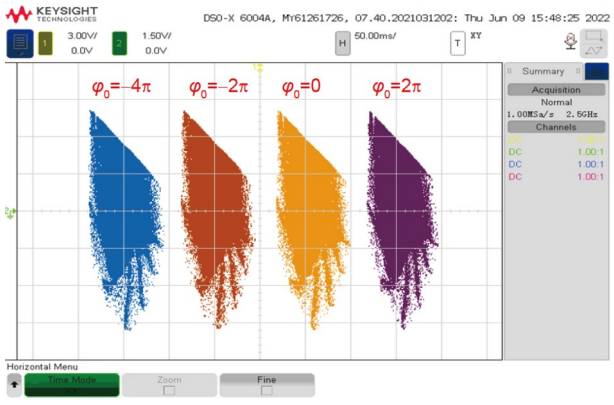

Figure 9 Experimentally acquired hyperchaotic attractors from the ID-Rulkov neuron model for $\alpha = 5$, $\sigma = 0.2$, $\varepsilon = 0.3$, $k = -0.5$, and $(x_0, y_0) = (0, 0)$, which demonstrate the amplitude-controllable hyperchaos boosted by the memristor initial value.

[0,1] can be obtained by operating modulo 1 to X. Subsequently, each output $Y(n)$ is converted into 52-bit binary stream $Y_B(n)$ using the IEEE 754 float standard. Thus, the sequences from the 35th to the 42nd in each binary stream are considered as PRNs, and they can be expressed as

$$P_i = Y_B(n)_{35:42}. \tag{13}$$

Here, we consider the ID-Rulkov neuron model under two specific memristor initial values $\varphi_0 = 0$ and 2π as two examples, and the designed PRNGs are called PRNG1 and PRNG2, respectively.

4.2 Randomness test by NIST SP800-22

The National Institute of Standards and Technology (NIST) SP800-22 test suite [37] is utilized to measure the randomness of the designed PRNGs, which is a convinced random-number test standard that contains 15 subtests. Each subtest is designed to determine a nonrandom area within a set of binary sequences. Significance level γ is set to measure the statistical errors, and it is considered as 0.01. The bits of each binary sequence should not be smaller than 10^6. In our experiment, a set of 120 binary sequences with 10^6 bits is generated by each PRNG and measured using the NIST SP800-22 standard.

Each subtest generates a P-value for every binary sequence. Thus, 120 P-values are generated by each subtest, and they can indicate the measured result from the two aspects of pass rate and P-value$_T$. The pass rate indicates how many binary sequences have passed the subtest. The related binary sequence can pass the test if the P-value is not smaller than the threshold, which is 0.9628 for $\gamma = 0.01$, and 120 binary sequences according to the calculation in [37]. P-value$_T$ calculates the distribution of these generated P-values. It first counts the number of P-values that fall into each of the 10 uniformly divided sub-intervals within [0,1]. Then, a χ^2 test is performed on the numbers of P-values in every sub-interval and generates P-value$_T$. At P-value$_T$ that is larger than 0.0001, the related subtest can be passed [37]. Table 4 shows the NIST SP800-22 results of the binary sequences generated by the two PRNGs. It shows that these sequences can obtain pass rates and P-value$_T$s that are all larger than the thresholds of 0.9628 and 0.0001, which means that the ID-Rulkov neuron model can generate highly random PRNs. To save space, we only take the binary sequences generated by the ID-Rulkov neuron model under two specific memristor initial values as examples. In fact, the binary sequences generated by this model under other memristor initial values can also pass the test.

4.3 InfoEn evaluation

To compare the application performance of PRNs generated by the ID-Rulkov neuron model with some existing discrete

Table 4 NIST SP800-22 results of the binary sequences generated by two PRNGs

No.	Subtests	PRNG1 ($\phi_0 = 0$)		PRNG2 ($\phi_0 = 2\pi$)	
		Pass rate	P-value$_T$	Pass rate	P-value$_T$
		$\geqslant 0.9628$	$\geqslant 0.0001$	$\geqslant 0.9628$	$\geqslant 0.0001$
01	Freq.	0.9750	0.3242	0.9833	0.7728
02	Block Freq.	0.9917	0.2430	0.9917	0.8881
03	Cum. Sums[a)] (F)	0.9750	0.8623	0.9917	0.7399
	Cum. Sums[a)] (R)	0.9667	0.9885	0.9833	0.8623
04	Runs	0.9917	0.5681	0.9917	0.8755
05	Longest Runs	0.9833	0.3641	1.0000	0.8043
06	Rank	0.9750	0.2645	0.9667	0.3925
07	FFT	0.9833	0.6198	0.9917	0.5681
08	Non-Ovla. Temp.[a)]	0.9907	0.5019	0.9900	0.4445
09	Ovla. Temp.	1.0000	0.7887	1.0000	0.7728
10	Universal	0.9917	0.4846	0.9833	0.8195
11	Appr. Entropy	1.0000	0.8881	1.0000	0.8343
12	Ran. Exc.[a)]	0.9852	0.4039	0.9938	0.6445
13	Ran. Exc. Var.[a)]	0.9920	0.4796	0.9910	0.5298
14	Serial (1st)	0.9833	0.4846	1.0000	0.4220
	Serial (2nd)	0.9917	0.6718	1.0000	0.9997
15	Lin. complexity	1.0000	0.4373	0.9833	0.6718
	Success No.	15/15	15/15	15/15	15/15

systems, we generate PRNs using the ID-Rulkov neuron model under the four specific memristor initial values listed in Table 2 and four existing 2D chaotic systems under their representative parameter and initial-value settings as the source chaotic system in eq. (13). The information entropy (InfoEn) is used to evaluate the distribution of these PRNs.

InfoEn is a well-known indicator for testing the distribution of a signal. For signal P, its InfoEn is calculated as

$$H(P) = -\sum_{i=1}^{2^n} p(P_i)\log_2 p(P_i), \tag{14}$$

where P_i indicates the ith possible value in signal P, $p(P_i)$ represents the probability, and n is the bit length of each value. Every 8 bits of PRNs are used as a value in our experiment. Then, we can obviously see that the maximum InfoEn is eight when all the possible values are equally distributed. Larger InfoEn means more uniform distribution of PRNs.

Table 5 lists the InfoEns of the eight PRNs with 10000-bit lengths provided by the different chaotic systems. These existing chaotic systems include the Hénon map [38], CF_a map with curve fixed points [39], hidden NFI_a map [40], and NEM_1 quadratic map [41]. These representative parameter and initial-value settings are set in reference to [24]. Obviously, PRNs obtained from the ID-Rulkov neuron model can obtain larger InfoEns than those from the four existing 2-D chaotic systems, which indicates that the hyperchaotic sequences provided by the ID-Rulkov neuron model are more uniformly and randomly distributed. When used in many practical applications, PRNs are required to show high randomness. Thus, the ID-Rulkov neuron model can produce PRNs that show better performance in these applications. In addition, PRNs generated by the ID-Rulkov neuron model under the four specific memristor initial values exhibit almost the same InfoEn, which further illustrates that the hyperchaotic sequences provided by the ID-Rulkov neuron model can be nondestructively boosted by the initial value of the memristor.

5 Conclusions

Intracellular ion pumping is random and paroxysmal, and the electromagnetic field is variable. Meanwhile, magnetic flux is a statistical scalar, and the transient effects are missed when continuous models are used. Thus, the combination of memristor and discrete map can reliably demonstrate the biophysical effects of neurons and nervous systems. This paper proposes an ID-Rulkov neuron model using the aforementioned principle to better characterize the electromagnetic induction effect. The memristor-induced stability effects are briefly evaluated by detecting the period-doubling and Neimark-Sacker bifurcation routes. The memristor-induced dynamical effects on the ID-Rulkov neuron model are numerically investigated using bifurcation plots and firing patterns, and the memristor initial-boosting mechanism of the infinite coexisting patterns is theoretically expounded. The results reveal that the ID-Rulkov neuron model exhibits complex dynamics, including memristor parameter-related bifurcation and memristor initial-boosting behavior. Its generated hyperchaotic attractors, which are verified by hardware experiments, can be nondestructively boosted by the initial value of the memristor. Compared with the continuous neuron model, the ID-Rulkov neuron model generates hyperchaotic sequences with lower dimensions and provides random numbers with higher randomness, which can be easily implemented on a digital hardware platform. Owing to their excellent performance, the nondestructively boosted hyperchaotic sequences can be used in various chaos-based applications such as image encryption [42], PRNG [43], secure communication [44], and generative adversarial nets [45]. This subject deserves further study.

Table 5 InfoEn evaluations of PRNGs provided by different chaotic systems

ID-Rulkov model	$\varphi_0 = -4\pi$	$\varphi_0 = -2\pi$	$\varphi_0 = 0$	$\varphi_0 = 2\pi$
$H(P)$	7.9970	7.9963	7.9965	7.9964
Existing 2D maps	Hénon map	CF_a map	NFI_a map	NEM_1 map
$H(P)$	7.9578	7.2207	6.9811	6.8540

This work was supported by the National Natural Science Foundation of China (Grant Nos. 62271088 and 62201094) and the Scientific Research Foundation of Jiangsu Provincial Education Department, China (Grant No. 22KJB510001).

1 Shilnikov A L, Rulkov N F. Origin of chaos in a two-dimensional map modeling spiking-bursting neural activity. Int J Bifurcation Chaos, 2003, 13: 3325–3340
2 Hodgkin A L, Huxley A F. A quantitative description of membrane current and its application to conduction and excitation in nerve. J Physiol, 1952, 117: 500–544
3 Rajamani V, Kim H, Chua L. Morris-Lecar model of third-order barnacle muscle fiber is made of volatile memristors. Sci China Inf Sci, 2018, 61: 060426
4 Chua L. If it's pinched it's a memristor. Semicond Sci Technol, 2014, 29: 104001
5 Eshraghian K, Kavehei O, Cho K R, et al. Memristive device fundamentals and modeling: Applications to circuits and systems simulation. Proc IEEE, 2012, 100: 1991–2007
6 Bao H, Chen Z G, Cai J M, et al. Memristive cyclic three-neuron-based neural network with chaos and global coexisting attractors. Sci China Tech Sci, 2022, 65: 2582–2592
7 Chen C, Min F, Zhang Y, et al. Memristive electromagnetic induction effects on Hopfield neural network. Nonlinear Dyn, 2021, 106: 2559–2576
8 Ma J, Yang Z, Yang L, et al. A physical view of computational neurodynamics. J Zhejiang Univ Sci A, 2019, 20: 639–659
9 Corinto F, Forti M. Memristor circuits: Bifurcations without parameters. IEEE Trans Circuits Syst I, 2017, 64: 1540–1551
10 Hong Q, Chen H, Sun J, et al. Memristive circuit implementation of a self-repairing network based on biological astrocytes in robot appli-

cation. IEEE Trans Neural Netw Learn Syst, 2022, 33: 2106–2120
11 Li K, Bao H, Li H, et al. Memristive rulkov neuron model with magnetic induction effects. IEEE Trans Ind Inf, 2022, 18: 1726–1736
12 Zhong Y, Tang J, Li X, et al. Dynamic memristor-based reservoir computing for high-efficiency temporal signal processing. Nat Commun, 2021, 12: 408
13 Hua L, Zhu H, Shi K, et al. Novel finite-time reliable control design for memristor-based inertial neural networks with mixed time-varying delays. IEEE Trans Circuits Syst I, 2021, 68: 1599–1609
14 Mannan Z I, Adhikari S P, Yang C, et al. Memristive imitation of synaptic transmission and plasticity. IEEE Trans Neural Netw Learn Syst, 2019, 30: 3458–3470
15 Kumar S, Strachan J P, Williams R S. Chaotic dynamics in nanoscale NbO_2 Mott memristors for analogue computing. Nature, 2017, 548: 318–321
16 Lin P, Li C, Wang Z, et al. Three-dimensional memristor circuits as complex neural networks. Nat Electron, 2020, 3: 225–232
17 Bilotta E, Pantano P, Vena S. Speeding up cellular neural network processing ability by embodying memristors. IEEE Trans Neural Netw Learn Syst, 2017, 28: 1228–1232
18 Lv M, Wang C, Ren G, et al. Model of electrical activity in a neuron under magnetic flow effect. NOnlinear Dyn, 2016, 85: 1479–1490
19 Ma J, Tang J. A review for dynamics in neuron and neuronal network. Nonlinear Dyn, 2017, 89: 1569–1578
20 Bao B C, Zhu Y X, Ma J, et al. Memristive neuron model with an adapting synapse and its hardware experiments. Sci China Tech Sci, 2021, 64: 1107–1117
21 Ge M, Jia Y, Xu Y, et al. Mode transition in electrical activities of neuron driven by high and low frequency stimulus in the presence of electromagnetic induction and radiation. Nonlinear Dyn, 2018, 91: 515–523
22 Bao H, Gu Y, Xu Q, et al. Parallel bi-memristor hyperchaotic map with extreme multistability. Chaos Solitons Fractals, 2022, 160: 112273
23 Li H, Hua Z, Bao H, et al. Two-dimensional memristive hyperchaotic maps and application in secure communication. IEEE Trans Ind Electron, 2021, 68: 9931–9940
24 Bao H, Hua Z, Li H, et al. Discrete memristor hyperchaotic maps. IEEE Trans Circuits Syst I, 2021, 68: 4534–4544
25 Rulkov N F. Modeling of spiking-bursting neural behavior using two-dimensional map. Phys Rev E, 2002, 65: 041922
26 Rulkov N F. Regularization of synchronized chaotic bursts. Phys Rev Lett, 2001, 86: 183–186
27 Wagemakers A, Sanjuán M A F. Electronic circuit implementation of the chaotic Rulkov neuron model. J Franklin Institute, 2013, 350: 2901–2910
28 Bao H, Liu W, Ma J, et al. Memristor initial-offset boosting in memristive HR neuron model with hidden firing patterns. Int J Bifurcation Chaos, 2020, 30: 2030029
29 Kim J, Pershin Y V, Yin M, et al. An experimental proof that resistance-switching memory cells are not memristors. Adv Electron Mater, 2020, 6: 2000010
30 Pershin Y V, Kim J, Datta T, et al. An experimental demonstration of the memristor test. Physica E, 2022, 142: 115290
31 Lu L L, Yi M, Liu X Q. Energy-efficient firing modes of chay neuron model in different bursting kinetics. Sci China Tech Sci, 2022, 65: 1661–1674
32 Lv M, Ma J, Yao Y G, et al. Synchronization and wave propagation in neuronal network under field coupling. Sci China Tech Sci, 2019, 62: 448–457
33 Bao H, Chen M, Wu H G, et al. Memristor initial-boosted coexisting plane bifurcations and its extreme multi-stability reconstitution in two-memristor-based dynamical system. Sci China Tech Sci, 2020, 63: 603–613
34 Bandt C, Pompe B. Permutation entropy: A natural complexity measure for time series. Phys Rev Lett, 2002, 88: 174102
35 Theiler J. Efficient algorithm for estimating the correlation dimension from a set of discrete points. Phys Rev A, 1987, 36: 4456–4462
36 Bakiri M, Guyeux C, Couchot J F, et al. A hardware and secure pseudorandom generator for constrained devices. IEEE Trans Ind Inf, 2018, 14: 3754–3765
37 Rukhin A L, Soto J, Nechvatal J, et al. A statistical test suite for random and pseudorandom number generators for cryptographic applications. Special Publication (NIST SP). Gaithersburg: National Institute of Standards and Technology, 2010
38 Rong K, Bao H, Li H, et al. Memristive Hénon map with hidden Neimark-Sacker bifurcations. Nonlinear Dyn, 2022, 108: 4459–4470
39 Jiang H, Liu Y, Wei Z, et al. A new class of two-dimensional chaotic maps with closed curve fixed points. Int J Bifurcation Chaos, 2019, 29: 1950094
40 Jiang H, Liu Y, Wei Z, et al. Hidden chaotic attractors in a class of two-dimensional maps. Nonlinear Dyn, 2016, 85: 2719–2727
41 Panahi S, Sprott J C, Jafari S. Two simplest quadratic chaotic maps without equilibrium. Int J Bifurcation Chaos, 2018, 28: 1850144
42 Bao H, Hua Z Y, Liu W B, et al. Discrete memristive neuron model and its interspike interval-encoded application in image encryption. Sci China Tech Sci, 2021, 64: 2281–2291
43 Hua Z Y, Zhou B H, Zhang Y X, et al. Modular chaotification model with FPGA implementation. Sci China Tech Sci, 2021, 64: 1472–1484
44 Zhang L, Chen Z, Rao W, et al. Efficient and secure non-coherent ofdm-based overlapped chaotic chip position shift keying system: Design and performance analysis. IEEE Trans Circuits Syst I, 2020, 67: 309–321
45 Bao H, Hua Z, Li H, et al. Memristor-based hyperchaotic maps and application in auxiliary classifier generative adversarial nets. IEEE Trans Ind Inf, 2022, 18: 5297–5306